Title

The magnitude and pace of photosynthetic recovery after wildfire in California ecosystems

Journal

Proceedings of the National Academy of Sciences of the United States of America, 120(15)

ISSN

0027-8424

Authors

Hemes, Kyle S
Norlen, Carl A
Wang, Jonathan A
et al.

Publication Date

2023-04-11

DOI

10.1073/pnas.2201954120

Peer reviewed

PNAS RESEARCH ARTICLE | ENVIRONMENTAL SCIENCES SUSTAINABILITY SCIENCE OPEN ACCESS

The magnitude and pace of photosynthetic recovery after wildfire in California ecosystems

Kyle S. Hemes[a,1], Carl A. Norlen[b,c], Jonathan A. Wang[b], Michael L. Goulden[b], and Christopher B. Field[a]

Edited by Janet Franklin, University of California, Riverside, CA; received February 2, 2022; accepted January 26, 2023

Wildfire modifies the short- and long-term exchange of carbon between terrestrial ecosystems and the atmosphere, with impacts on ecosystem services such as carbon uptake. Dry western US forests historically experienced low-intensity, frequent fires, with patches across the landscape occupying different points in the fire-recovery trajectory. Contemporary perturbations, such as recent severe fires in California, could shift the historic stand-age distribution and impact the legacy of carbon uptake on the landscape. Here, we combine flux measurements of gross primary production (GPP) and chronosequence analysis using satellite remote sensing to investigate how the last century of fires in California impacted the dynamics of ecosystem carbon uptake on the fire-affected landscape. A GPP recovery trajectory curve of more than five thousand fires in forest ecosystems since 1919 indicated that fire reduced GPP by 157.4 ± 7.3 g C m^{-2} y^{-1}(mean ± SE, n = 1926) in the first year after fire, with average recovery to prefire conditions after ~12 y. The largest fires in forested ecosystems reduced GPP by 393.8 ± 15.7 g C m^{-2} y^{-1} (n = 401) and took more than two decades to recover. Recent increases in fire severity and recovery time have led to nearly 9.9 ± 3.5 MMT CO_2 (3-y rolling mean) in cumulative forgone carbon uptake due to the legacy of fires on the landscape, complicating the challenge of maintaining California's natural and working lands as a net carbon sink. Understanding these changes is paramount to weighing the costs and benefits associated with fuels management and ecosystem management for climate change mitigation.

wildfire | carbon uptake | regeneration | GPP

Significance

Forests' capacity to absorb atmospheric CO_2 through vegetation growth (carbon uptake) depends in part on how long it has been since, and the severity of, wildfire. Increases in fire area and severity, as observed in California recently, could change both CO_2 released into the atmosphere and the cumulative forest carbon uptake. We combine ground measurements and satellite observations to understand how fire has changed carbon uptake across California over the past century. We find that the recent increase in fire area and severity has reduced carbon uptake, compared to unburned and overstocked controls. Active management that enhances ecosystem resilience and decreases future fire severity may accelerate the recovery of carbon uptake following fire.

Wildfire has the ability to greatly modify the short- and long-term fluxes of carbon between the land surface and the atmosphere (1), impacting the provisioning of key ecosystem services from natural lands upon which society relies (2). Globally, fire emissions of 2.2 Pg C y^{-1}—the equivalent of more than a fifth of global fossil fuel emissions in 2019 (3)—transfer large amounts of carbon from vegetative carbon pools to the atmosphere (4, 5). In the past, assumption of a fire–climate equilibrium provided a convenient framework to account for legacy effects of fire on climate (4). In a closed system at steady state, fire emissions of CO_2 are compensated by net carbon uptake from forest stands in different stages of postfire regeneration, making the impact of fires on carbon budgets neutral over decadal timescales at large scales (4–7). This assumption holds only if fire area and severity—and thus fire CO_2 emissions—stay relatively stationary (1). When severe enough to be lethal to vegetation, increasing fire area will skew the age distribution of vegetation toward younger age classes; decreasing fire area will result in a distribution with older age classes. Globally, a combination of disturbance, land use change, and climate change has pushed forests toward younger age classes over the last century, potentially resulting in a net change in carbon uptake (2).

Increasingly severe fires in forests are particularly concerning because of the important role that forests and forest regeneration play in climate regulation (8). While historically low-intensity, frequent fires in dry western North American forests (including indigenous anthropogenic burning) presumably reached a nearly steady state with respect to climate, contemporary changes to disturbance rate and intensity have altered the carbon cycle across the landscape. The fire regimes of the forests of the western United States have been greatly modified by a nearly century-long policy of fire suppression (9–12), leading to overstocked forests and shifts in size distributions and species composition (13–15). Interacting with these dynamics, anthropogenic climate change is making large, high-severity fires more common (16–18) and potentially reducing biomass carrying capacity on the landscape (2, 19–22). In addition, warmer and drier climatic conditions following severe fires are limiting tree seedling recruitment and regeneration across the western United States, further reducing the capacity of fire-prone forests to take up and store

Author contributions: K.S.H., C.A.N., J.A.W., M.L.G., and C.B.F. designed research; K.S.H., C.A.N., and J.A.W. performed research; K.S.H., C.A.N., and J.A.W. analyzed data; and K.S.H., C.A.N., J.A.W., M.L.G., and C.B.F. wrote the paper.

The authors declare no competing interest.

This article is a PNAS Direct Submission.

[1]To whom correspondence may be addressed Email: khemes@stanford.edu.

This article contains supporting information online at http://www.pnas.org/lookup/suppl/doi:10.1073/pnas.2201954120/-/DCSupplemental.

Published April 3, 2023.

carbon (23–26). A changing fire regime and slowed postdisturbance regeneration could lead to reductions in cumulative carbon uptake across the fire-impacted landscape.

California is a prime example of many of these challenges—experiencing a majority of its largest modern fires in the last half decade (27–29). Over the past century, fire suppression and other management practices have led to California's forests becoming denser, with more small trees, less overall basal area, and altered species composition (13, 14). Due to the changing forest structure, along with hotter, drier conditions, and shorter wet seasons, the area and severity of wildfire (often highly correlated) have greatly increased (*SI Appendix*, Fig. S1) (28). Understanding how this contemporary wildfire regime has changed the legacy of carbon uptake on the landscape is critical to weighing the costs and benefits of wildfire fuels management and to account for wildfire impacts on California's ambitious climate change mitigation goals (30), which seek to maintain natural and working lands as a net carbon sink (31). We define "foregone carbon uptake" as the cumulative impact of reduced productivity of burned lands compared to unburned, matched control pixels. Because of a long history of fire suppression and forest management throughout California, the unburned control areas do not represent a stable, "natural," or even desirable baseline state. Instead, the comparison allows us to compare the GPP in recovering fire perimeters with that in an otherwise similar forest.

We set out to understand how the legacy of the last century of California fires has impacted carbon uptake. Our aim was to understand the first-order spatial patterns across a diverse array of wildland ecosystems that comprise California. Previous work has taken a space-for-time approach, with "snapshots" of eddy covariance-measured ecosystem-scale productivity at differently aged forests (32–34) or has observed ground-based recruitment and species mix at a small sample of fires, usually at the plot or patch scale (e.g., refs. 24, 35, 36). However, due to the stochastic nature of fire ignitions, these approaches are unable to capture a complete regional-scale estimate of the impact of fires. To obtain a more comprehensive picture, we combine three decades of medium-resolution satellite data, 90 site-years of nearly continuous ecosystem-scale gross primary productivity (GPP) observations from a range (*SI Appendix*, Fig. S3) of California ecosystems and elevations and archival databases of the timing and burn perimeters of fires (*Materials & Methods*) to quantify the foregone carbon uptake of fires in California since 1919. We primarily utilize the State of California's exhaustive Fire and Resource Assessment Program (FRAP) dataset of historical California fire perimeters. We supplement this with the United States Forest Service (USFS) Vegetation Burn Severity dataset, which contains a subset of the FRAP fires, split into normalized burn severity polygons (37) (*Materials & Methods*). We align fires by "years since fire" or recovery age to observe a broad range of recovery periods.

We use this analysis to ask the following: 1) What is the magnitude and spatial arrangement of foregone carbon uptake associated with recent fires in California? 2) How long does it take for recently burned areas to recover carbon uptake capacity to that of unburned controls? 3) How has postfire carbon uptake recovery changed over recent decades? Satellite-based multispectral proxies of GPP are well established (e.g., ref. 38). In particular, a multispectral index of near-infrared reflectance (NIRv) has been shown to serve as an effective proxy for light capture, integrating aspects of canopy structure that control photosynthetic uptake (39–42). We focus on gross carbon uptake as an ecosystem service, as opposed to net carbon uptake, which depends on high-confidence measurement or modeling of ecosystem respiration, for which there are weaker proxies (38). Our method allows us to quantify the carbon uptake legacy of fire disturbance across broader spatial and temporal scales than previous work. It also facilitates placing the legacy of wildfires in the context of established theories of forest succession (43) and management strategies into the future.

Results

Across the more than 5,000 fires (*SI Appendix*, Fig. S1) that we analyzed from California forests since 1984 (27), annual GPP fell 16.5 ± 0.5 % (mean ± SE,n= 1988) in the year after fire, but with substantial variability between and within fires and between years (Fig. 1*A*). Based on comparisons with a set of undisturbed control pixel bins (*Materials & Methods* and *SI Appendix*, Figs. S2 and S4), a fire's impact on GPP (dGPP) was usually (68.5% of all fires that occurred in predominantly forestland) negative immediately postfire (Fig. 1*B*), indicating a reduction in photosynthetic carbon uptake capacity related to vegetation and leaf area lost in the disturbance (*SI Appendix*, Fig. S5). The mean California forest wildfire (Fig. 2*A*) reduced GPP by 157.4 ± 7.3 g C m^{-2} y^{-1} (mean ± SE,n= 1926) in the first year after fire, with average recovery to prefire conditions after ~12 (10 to 12) y. About half of fires recovered carbon uptake capacity within the first decade after fire. This reflects the fact that the majority of fires in California are of low severity, are small (especially due to the policy of fire suppression; *SI Appendix*, Fig. S1), and have relatively short-lived effects. The other half of fires in predominately forested ecosystems still experienced a persistent GPP reduction, compared to unburned controls, a decade postfire. After recovery of GPP—which we define as the time at which dGPP flips from negative to positive—along with the range of crossover considering the CI, many fires exhibited enhanced uptake before trending back toward an undisturbed equilibrium (Fig. 2*A*).

The historical predominance of small fires in California can mask the implications of the more severe, larger forest fires characteristic of the last two decades (18, 28) (*SI Appendix*, Fig. S1), in which the average acre burned more intensely. In forest-dominated fires, the largest magnitude and longest-lasting GPP reductions occurred following the largest quintile of fires −393.8 ± 15.7 g C m^{-2} y^{-1}; 20 y (20 to 30); (n = 401) and fires in the wettest quintile of climates (−234.8 ± 17.0 g C m^{-2} y^{-1}; 21 y (19 to 24); (n = 348)) (Fig. 2 *B* and *E*). We used USFS fire polygons (37), partitioned by normalized burn severity across fires and years, to determine the impact of fire severity on GPP recovery (Fig. 3*A*). The most severe burn areas in this dataset resulted in −613.6 ± 10.4 g C m^{-2} y^{-1} (n = 916 polygons) in the first year since fire, compared to the least severe fires which experienced an initial GPP reduction of −214.4 ± 8.8 g C m^{-2} y^{-1}; (n = 1262 polygons).

Burn severity leads to different amounts of foregone carbon uptake depending on the forest type. High-severity burns led to a large initial GPP reduction in the wetter Coastal Range, Cascades, and Klamath ecozones, compared to the drier Sierra Nevada, or Southern California Mountains (Fig. 3*B*). Across the entire population of FRAP fires, postfire GPP reductions tended to be larger in northern California, where forest carbon stocks are greater, and climate is wetter than the statewide average. In Southern California, where frequent and relatively low-severity

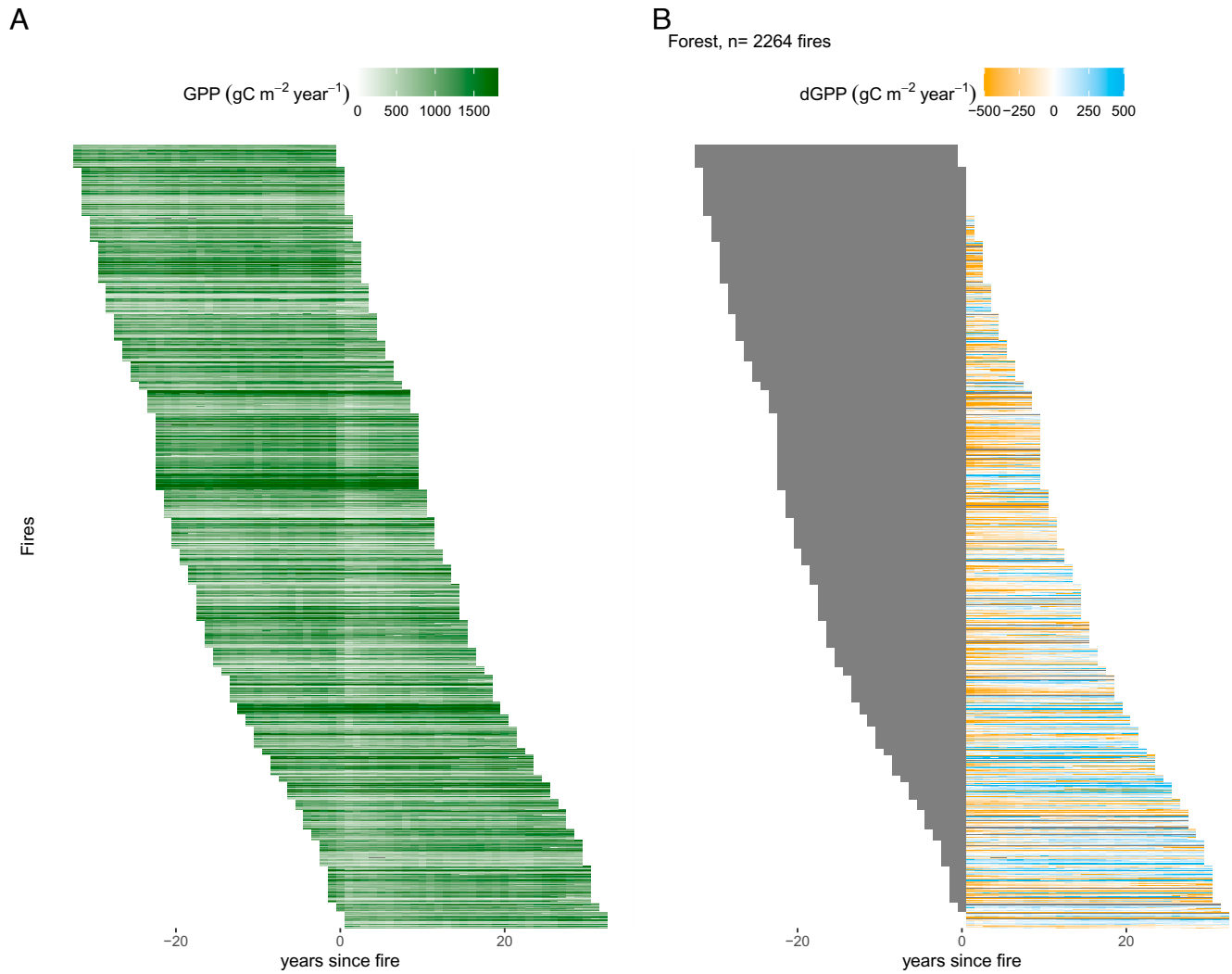

Fig. 1. GPP (*A*) and change in GPP due to fire (dGPP) (*B*) across 2264 California fires that occurred in predominantly forested land cover types since 1984. Each fire (row) is aligned as a chronosequence (years since fire). dGPP is calculated by comparing postfire GPP to a set of recently undisturbed control pixels (*Materials & Methods*). (*SI Appendix*, Fig. S5 for forest fires since 1919).

shrub fires are more common, postfire GPP reductions were generally smaller, and recovery was faster, in many cases with GPP enhancements after just a few years (*SI Appendix*, Fig. S6).

To better understand the interactions among the complex set of drivers contributing to GPP recovery postfire, we utilized a generalized additive model with cubic spline smooths (*Materials & Methods*) to derive the partial effects of predictor variables (area, fire severity using percent dNBR change in the year postfire, mean temperature, mean precipitation, elevation, percent of the area that has reburned, prefire mean GPP, and fire start year) on dGPP at 10 y postfire (r^2 = 48.9%; all predictors significant) (*SI Appendix*, Fig. S7). Holding other explanatory variables constant, we derived residual response functions for each of the eight recovery predictors. Consistent with binned recovery curves (Fig. 2 *B*–*E*), fire disturbances with a large area (*A*), high severity (*B*), and in locations with relatively high average precipitation (*D*) each resulted in negative residuals, indicating the importance of these variables in driving GPP reductions compared to unburned controls a decade postfire. Residuals were also negative for low elevation and low prefire GPP.

By grouping recovery by decade, we identified a systematic fingerprint of the changing recovery trajectories over time, which may be responding to global change drivers such as increasing temperature and vapor pressure deficit. GPP recovery trajectories from forest-dominated fires in the 1980s experienced smaller postfire GPP reductions (1980s: -105.9 ± 19.4 g C m^{-2} y^{-1}, n = 264; 2010s: -183.9 ± 15.2 g C m^{-2} y^{-1} , n = 475) and faster recovery (1980s: 7 y (5 to 11); 2010s: 14 y (12 to 18) (Fig. 2*D*). On average, a stand one decade postfire in the 2010s still experienced a GPP reduction, while a similar stand age in the 1980s had recovered and exceeded the carbon uptake of its unburned baseline.

We used the cumulative enhancement and reduction of GPP over all fires since 1919, relative to the control pixels, to compute the state-wide area-weighted cumulative GPP impact of the past century of fire—what we call the landscape-scale fire legacy. Fire led to a small net enhancement in GPP on fire-disturbed lands during the 1980s. Over the last two decades, however, GPP decreased dramatically across California's fire-disturbed landscape compared to unburned controls, resulting in 9.9 ± 3.5 MMT CO_2 (3 y rolling mean and SE) of forgone carbon uptake due to the legacy of fires on the landscape as of 2018 (Fig. 4*C*). Most of this net reduction comes from fires in forests (Fig. 4*A*), with fires in shrub-dominated ecosystems leading to

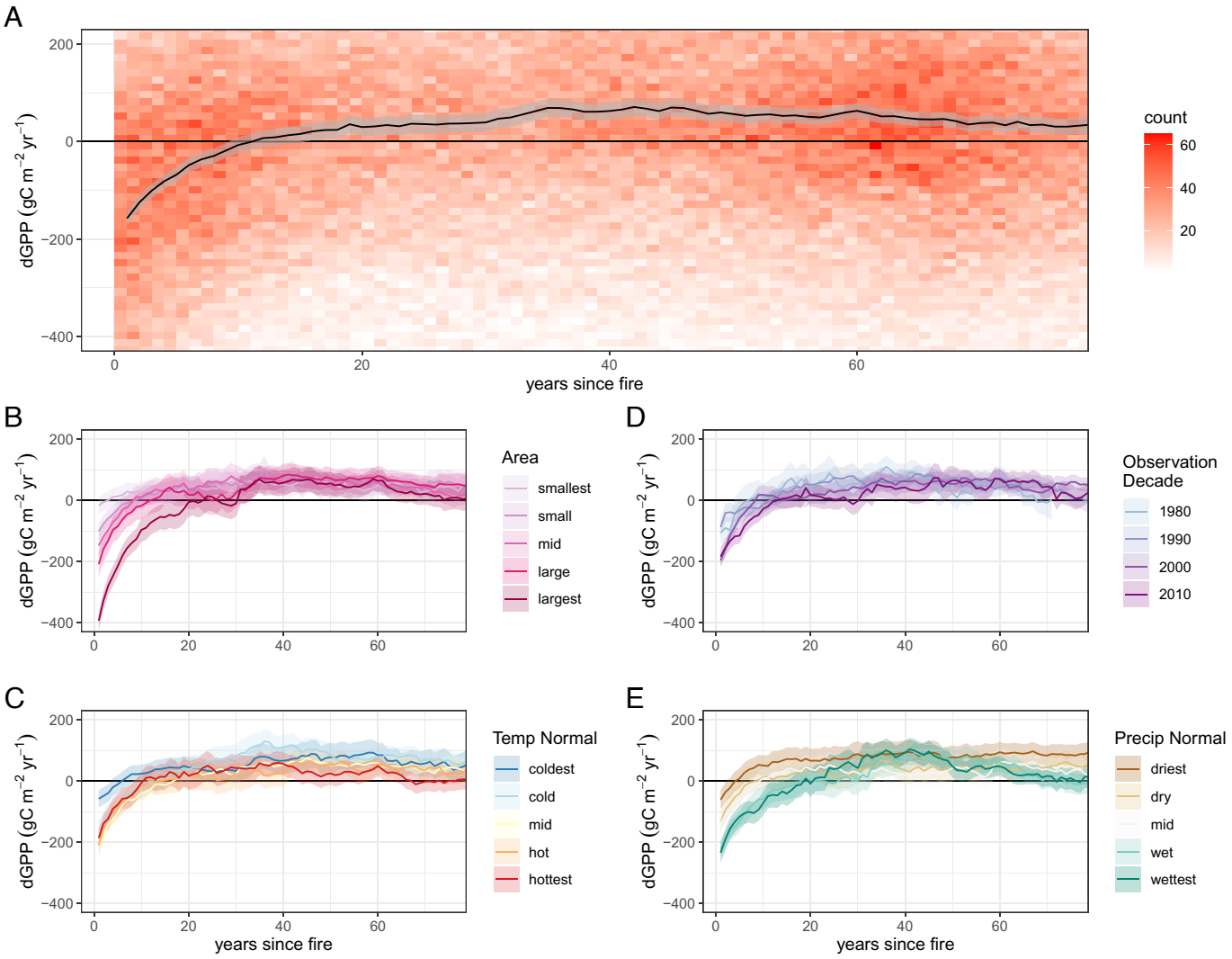

Fig. 2. Mean dGPP and CI in each year since fire for (*A*) all forest wildfires in California since 1919, binned by quintiles of (*B*) area, (*C*) 30-y (1981 to 2010) temperature, (*D*) decade of fire observation (note that the 1980 and 2010 decades are not complete; the 1980 decade includes 1984 to 1989 and the 2010 decade includes 2010 to 2018), and (*E*) 30-y (1981 to 2010) precipitation normals.

substantial variability in dGPP due to fire, but generally net equilibrium (Fig. 4*B*).

Discussion

The mean dGPP fire recovery curve (Fig. 2*A*) generally follows the idealized expectation of postdisturbance succession, based on the idea that after a disturbance, reductions in carbon uptake are followed by recovery through predisturbance equilibrium, toward a temporary period of enhancement, and then a gradual recovery to baseline conditions (43). In forests, this process occurs on multidecade to century timescales.

In the year after fire, GPP in forest-dominated ecosystems decreased by 157.4 ± 7.3 g C m^{-2} y^{-1} (mean $\pm$ SE, $n = 1926$, followed by rapid recovery to undisturbed baseline conditions after more than a decade. There was a small (maximum of 71.0 ± 9.0 g C m^{-2} y^{-1} at 42 y since fire) GPP enhancement that persisted to at least ~90 y (Fig. 2*A*). This medium-term GPP enhancement is broadly consistent with other chronosequences of long-lived ponderosa pine recovery, in which net primary production increased to a maximum between 70 and 100 y (34).

Our results are consistent with previous work and, due to the number and breadth of fires analyzed, may be more broadly applicable. Previous work at the ecosystem scale employed eddy covariance measurements of partitioned net ecosystem exchange snapshots, using a space for time approach (32–34). Amiro et al. (32) synthesized a chronosequence of ecosystem flux data from four fire disturbance sites in North America, finding that the boreal forest sites recovered carbon uptake capacity after about a decade, while a drier Arizona site appeared to be on a much longer trajectory. Goulden et al. (33) likewise found relatively short-term (~2 decade) suppression of GPP following fire but noted that boreal forest recovery, facilitated by quickly resprouting herbs and shrubs, may be much faster than in water-limited southwestern forests that are not adapted to high-severity crown fires.

Evidence for this slow postfire GPP recovery in the southwest United States was supported by data from a severely burned ponderosa pine forest, where a decade following stand-replacing fire, the burned site's GPP was approximately 43% of an unburned control (45). Despite lower ecosystem respiration than a control site, the burned site was still a net source of CO_2 to the atmosphere. More recent landscape-scale work at coarser resolution looked at postfire recovery of GPP over large fires in

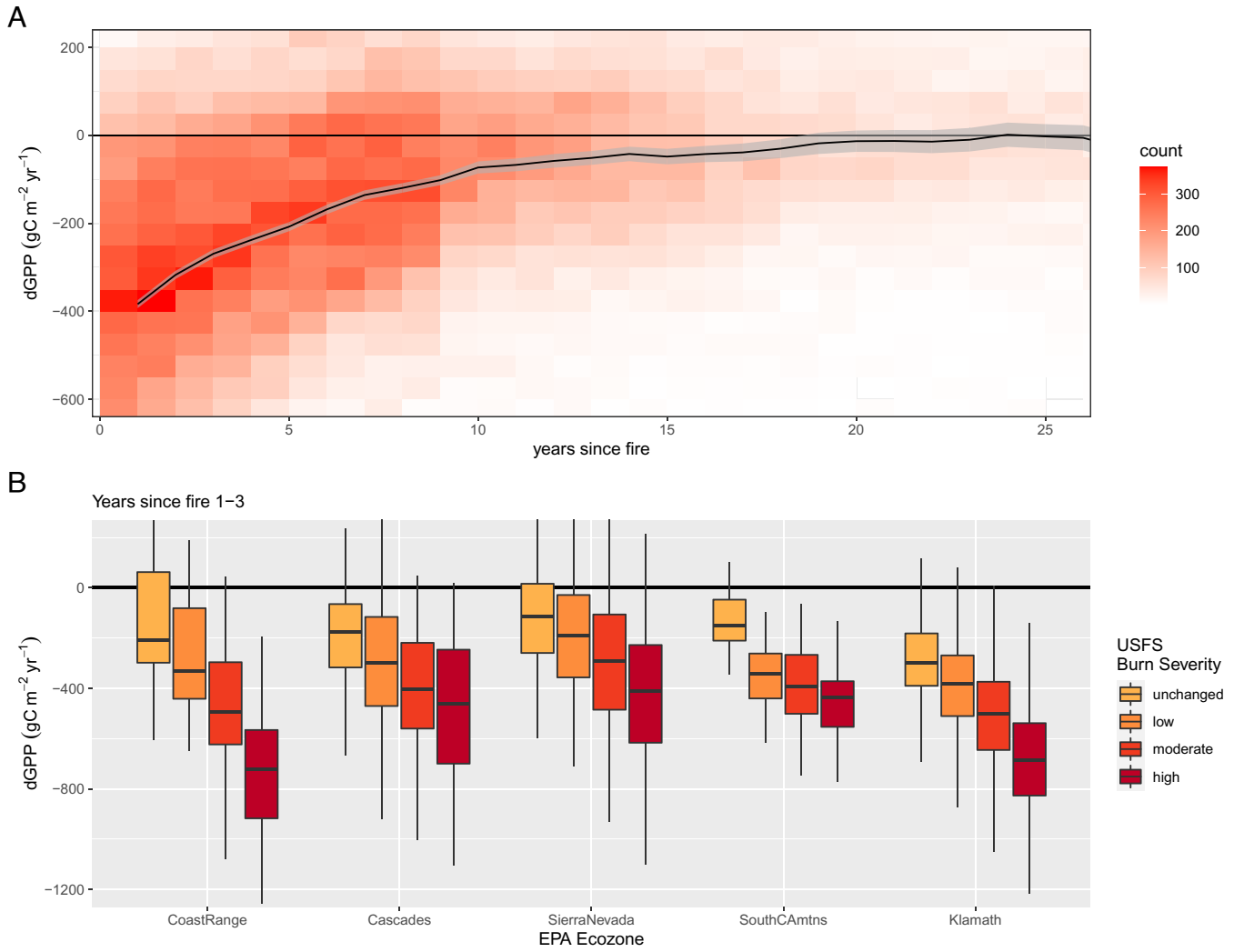

Fig. 3. Mean dGPP and CI in each year since for (*A*) USFS burn severity polygons and (*B*) separated by burn severity class.

the Western United States, finding GPP reductions that stabilized after 2 to 12 y postfire, except in the case of higher-severity fires (46). We found that forests took about a decade to recover carbon uptake capacity, on average, following a fire, which is consistent with these other studies. Furthermore, we observe that forests that experienced larger fires, in wetter sites, take substantially longer to recover (i.e., more than two decades at least).

California's contemporary fire regime is causing a growing cumulative GPP reduction in fire-affected landscapes, compared to otherwise similar unburned and overstocked controls. As recently as the end of the 1980s, the cumulative area-weighted GPP effect of California wildfires was near-neutral, meaning that the landscape-scale fire legacy was in equilibrium, summed across the population of patches in postfire regeneration (Fig. 4*C*). Since the turn of the century, however, the net GPP reduction of forest fire-affected areas has increased rapidly (Fig. 4*A*) to -14.6 ± 2.5 MMT CO_2 by 2017. Initial postfire GPP reductions are growing, and GPP recovery is slowing; postfire recovery trajectories for forest-dominated wildfires recovering in the 2010s were ∼7 y longer than the mean for fire in the 1980s. These changes have led to a reduction of carbon uptake on the fire-affected landscape, dominated by fires in predominantly forested ecosystems (Fig. 4*A*). Though not directly comparable, the magnitude of this foregone carbon uptake is similar, in some recent years, to the immediate CO_2 emissions from wildfire biomass incineration (shown for comparison in the unfilled bars of Fig. 4*C*) (44).

This landscape-scale foregone carbon uptake is a function of both larger, higher-severity fires and a slower pace of recovery, especially in the last two decades. This signal is also interwoven with impacts of CO_2 fertilization (47), hotter and drier conditions (21, 48), and prolonged droughts (49). The evidence for challenging recruitment and the potential for ecosystem state-changes after high-severity fires is also increasing, with the clearest signals from water-limited forests adapted to low-severity fire (23, 35). In past research, regeneration after severe fire in the mixed conifer/mixed evergreen forests of the Klamath Mountains was characterized by substantial competition and short (∼4 y) windows for recruitment, leading to protracted multidecadal recovery when immediate recruitment was inhibited (24). In a severely climate-changed California, large, severe fires in combination with chronic drought and disease could serve to catalyze wholesale biome shifts (48).

This study documents a shift in the effect of California's fire regime on cumulative GPP across the fire-affected landscape, from net enhancement to net reduction over the last several decades. Four considerations help put this result in context. First, the effect on GPP does not necessarily translate directly to

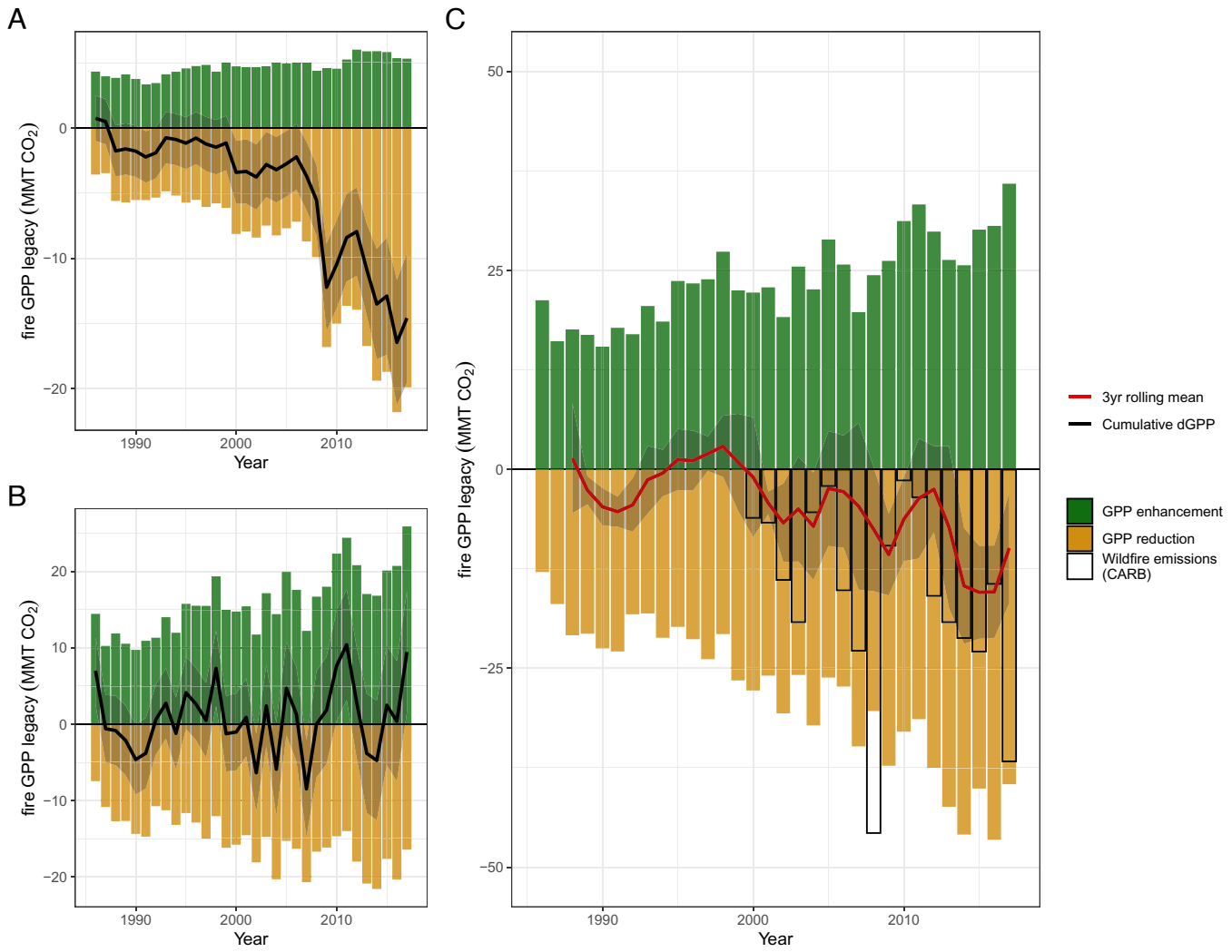

Fig. 4. Landscape scale fire GPP legacy and confidence intervals for (*A*) forest-dominated fires, (*B*) shrub-dominated fires, and (*C*) all California fires since 1919. To indicate multiyear trends in (*C*), the red line and shading represent the three-year rolling mean and CI of cumulative dGPP. Wildfire emissions (empty rectangles) are from the California Air Resources Board (44).

landscape-scale carbon balance. While we estimate the trajectory of carbon gains through GPP, we do not estimate carbon releases through direct combustion and ecosystem respiration. In many cases, fire alters the long-term trajectory of soil respiration, through mineralizing or protecting soil carbon and other nutrient pools (32, 50, 51). In an Oregon ponderosa pine chronosequence, however, soil-dominated heterotrophic respiration did not vary substantially with stand age (34). The trajectory of ecosystem respiration following fire depends on the quantity of dead biomass not consumed in the combustion. Measurements of carbon consumption in prescribed Sierra Nevada fires have demonstrated substantial surface fuel carbon consumption (52), while others have shown that common assumptions underestimate the amount of remaining biomass after fire (53). To build a more complete picture of the impact of fires on regional carbon balance, further research should examine changes in ecosystem respiration or net carbon storage following disturbance.

Second, our approach focuses on ecosystem function and does not provide information regarding the species mix or life form of the regenerating ecosystem. Rapid recovery of GPP could reflect regrowth of the species originally present and/or species of a similar life form, or it could indicate a transition to fast-growing early successional species of a different life form, like shrubs (54). Recent work on vegetation transitions in California points to a postfire trend toward denser, smaller, and more oak-dominated forests (14, 22). California forests, including their fire adaptations and fire tolerance, are diverse. Future work could disentangle the relative recovery patterns according to dominant species assemblages, allowing managers to understand which California forests are most at risk of delayed GPP recovery after high-severity wildfire, and how changes in the spatial distribution of species may affect this in the future.

Third, our experimental design, based on averaging annual GPP over all pixels within a fire perimeter (or in the case of Fig. 3, USFS fire severity polygons) and comparing this with the mean GPP of ~200 of the most similar (based on normal temperature and precipitation, elevation, and latitude) undisturbed control pixels (*Materials & Methods*), has benefits and limitations. GPP recovery can be quite heterogeneous within a single fire perimeter; we do not resolve the recovery of, for example, unburned islands within fire perimeters or the severity impacts on different life forms within the fire perimeter. These could act as important seed sources that hasten forest recovery (e.g., ref. 55). We also do not consider postfire management such as salvage logging or active

replanting and shrub management. Both can dramatically impact the course of succession in mixed conifer California forests (56).

The primary benefit of comparing fires with unburned control pixels is to capture background changes in GPP related to CO_2 fertilization (2, 21) and interannual climate variability. The main limitation is that, due to the length of the Landsat record, we do not know the nonfire disturbance history of control pixels before 1984. If some of the pixels we selected as controls had experienced GPP-reducing disturbance (i.e., logging) before the beginning of the Landsat record, they could have GPP either higher or lower than truly undisturbed sites. And, of course, few, if any, locations in California represent a precolonial baseline due to cessation of indigenous management, pervasive harvesting, and fire exclusion for the last century (57). This means that our unburned control represents, in places that have experienced intensive management and fire suppression, an unsustainable and overstocked condition.

Due to over a century of fire suppression, California and the western United States have a large-scale, largely unmet need for fuel-reduction treatments in overstocked forests (57) to reduce the risks of future catastrophic wildfires. Implementation of widespread fuel-reduction treatments at scale, as called for in California's latest wildfire and forest resilience action plan (58), could contribute to reversing the growing GPP reductions on fire-effected landscapes, though these treatments come with their own short-term carbon costs (59–62). While we do not differentiate between "natural" (i.e., lightning ignition), human-ignited, and prescribed fires, we do find a much smaller reduction in carbon uptake, and a nearly instantaneous recovery, after relatively small fires (Fig. 2*B*). Using the USFS fire severity-focused dataset, we also find that lower-severity fires result in lower initial GPP reductions (Fig. 3*B*). These findings are broadly consistent with evidence of enhanced carbon stability and forest resilience when fire-adapted forests experience thinning (63–65). In addition to avoiding direct fire emissions and reducing understory fuel loads that lead to severe crown fires, fuel reduction through prescribed burns and thinning can reduce the multidecadal GPP reductions associated with catastrophic fires and enhance long-term carbon stocks by releasing large trees from competitive pressure from understory vegetation.

Finally, in addition to changing carbon uptake capacity, fire impacts other important ecosystem services such as climate, water, and human health. Here, we have focused exclusively on CO_2, but wildfires also emit CH_4, N_2O, aerosols, and precursors to ozone (5, 66), which can have diverse impacts on vegetation productivity (67, 68) and negative impacts on human health (69, 70). High-severity fires modify the surface energy balance (71, 72), often leading to higher surface temperatures and altered evapotranspiration, imperiling downstream water security (73), quality (74), and quantity (75). Soil nitrogen and carbon are generally reduced under frequent or severe fires, leading to less hospitable soil environments for aboveground productivity (50, 76). The diverse spatial and temporal scales of these impacts warrant closer analysis of multidecadal postfire legacies of ecosystem services as components of the complete impact of fire on the landscape.

In this work, we quantified the landscape-scale impact of the contemporary fire regime on California's carbon uptake over the last century, using an exhaustive fire disturbance dataset and a wall-to-wall remote sensing chronosequence. The impact of this changing fire regime on climate goes well beyond the incineration emission of biomass carbon to atmospheric CO_2. We document the legacy effect that the fire regime imprints on the landscape—leading to younger, less productive forests that, over the last few decades, have led to foregone carbon uptake of close to 10 MMT CO_2 across fire-disturbed California lands (Fig. 4). This trend has been compounded by larger, more severe fires and longer time to recovery, potentially exacerbated by the challenges of regeneration in a hotter and drier climate, complicating the challenge of maintaining California's natural and working lands as a net carbon sink (15). Our work suggests that forest management practices—such as prescribed low-severity burns aimed at reducing large, severe, wildfires (77)—not only preserve carbon stocks in live biomass but can slow the trend toward net GPP reductions on the fire-affected landscape. This work provides a unique window into evolving impacts of California's changing fire regime, and it points to the importance of integrating ecosystem service recovery into the management of California's natural and working lands.

Materials and Methods

Overview. The three main datasets used were 1) monthly Landsat surface reflectance index (NIRv); 2) data from nine eddy covariance flux tower sites across a range of California ecosystems, constrained with gridded radiation and temperature reanalysis products and gap-filled and summed to create an annual, statewide GPP product between 1985 and 2018; and 3) fire perimeter datasets that include a statewide 100+ year fire perimeter (FRAP) and a Landsat-era fire severity class perimeter dataset (USFS). We utilized a change detection algorithm, plus topographic and climate geospatial layers, to identify recently undisturbed control pixels that matched with our fire perimeters. We computed the impact of fire on GPP (dGPP) by subtracting the annual mean GPP of the spatial control pixels from annual mean values of GPP from within each fire perimeter. We indexed each fire observation by "year since fire," or recovery age, allowing us to construct a chronosequence that spans many decades, despite only 33 y of Landsat observations. For example, for fires that occurred in 1984, we were able to observe years 1 to 34 of recovery. But for fires that occurred before the Landsat record, say in 1970, we could observe recovery for years 14 to 48. In this way, we observed different portions of postfire recovery for different fires. Together, this allowed us to reconstruct a chronosequence, based on time since disturbance, that spans nearly a century.

Remote Sensing Data and Harmonization. We accessed the Tier 1 surface reflectance record from the Landsat series of Earth-observing satellites using Google Earth Engine (78). We used established algorithms to homogenize the Landsat 5 Thematic Mapper equivalent of Bands 1, 2, 3, 4, 5, and 7 from the Landsat 7 Enhanced Thematic Mapper+ and the Landsat 8 Operational Land Imager using established regression lines derived for the Continental United States (79). We then combined the scenes from the Landsat 5, 7, and 8 to create a 34-y chronosequence (1984 to 2018) (80). Landsat data were quality-controlled by removing pixels using the USGS "pixel qa" mask based on FMask (81) to remove snow, clouds with high confidence, and cloud shadows from each Landsat scene. We calculated the mean Tasseled Cap Brightness (82) for the full Landsat stack and removed pixels from each Landsat scene that were anomalously (two SDs) bright (clouds or snow) or dark (shadows). For months in which we had no quality-controlled Landsat data (usually wintertime), we gap-filled using a harmonic fit to the monthly values.

NIRv, an effective proxy for light capture that integrates aspects of canopy structure that control photosynthetic uptake, was computed as the product of near-infrared reflectance (NIR) and the normalized difference vegetation index (NDVI) ($NIRv = NIR * ((NIR - Red)/(NIR + Red))$ (39, 40). The normalized burn ratio (NBR) was used as a proxy for fire severity and computed as the normalized difference of short-wave infrared reflectance (SWIR2) and near-infrared reflectance ($NBR = (NIR - SWIR2)/(NIR + SWIR2)$) (83). For *SI Appendix*, Fig. S7, we used the percent difference in mean NBR between the year before and the year after the fire burn year to determine fire severity.

Additional Geospatial Layers. We extracted supplementary geospatial layers over California to assist in interpreting results. These included topographic elevation, aspect, and slope (USGS National Elevation Dataset courtesy of the US Geological Survey; https://www.usgs.gov/core-science-systems/national-geospatial-program/national-map). We used 1981-2010 "PRISM" precipitation (water-year sum) and temperature (water-year average of monthly maximum temperature) (84), downscaled to 30 m. Though this product does not exactly overlap with our observation period (1984 to 2018), the size of the quantile bins used (Fig. 2) is much larger than the change in precipitation and temperature associated with climate change over that period, so we do not expect changes in climate during 2010 to 2018 to significantly influence our bins. We used the Landsat-based eMapr 1987 to 2018 land cover product to determine prefire landcover type (85), assigning pre-1987 fires to the dominant 1987 landcover type. Wildfire emissions are from the California Air Resources Board (44) (https://ww2.arb.ca.gov/wildfire-emissions).

California Flux Tower Scaling. The eddy covariance method represents the only continuous (measured at 10 to 20 Hz) ecosystem-scale (meaning integrated over a spatial footprint of $\sim$1 km^2) measurement of net CO_2 flux. The continuous temporal resolution (averaged to 30-min data) allows us to capture seasonal variation and interannual variability integrated across an assemblage of plant functional types (depending on the species in the measurement footprint). We leveraged a network of nine eddy covariance flux sites–together representing 90 site-years of data–across multiple California ecosystems and elevations (49, 86), along with the Landsat record, to translate the near-infrared vegetation index (NIRv) into gross primary production (GPP) at the 30-m scale over the past 34 y (*SI Appendix*, Fig. S3).

The eddy covariance flux sites share the same instrumentation, data processing, and maintenance (87). The eddy covariance systems include a closed-path infrared gas analyzer (LI-7000, LiCor Biosciences) and a 3D sonic anemometer(CSAT-3, Campbell Scientific). Data are corrected for sensor lag, mean wind rotation, and energy budget closure. At each eddy covariance site, we measured the net ecosystem exchange at 10 to 20 Hz, partitioned this into GPP and respiration using light-response curves fit during periods with sufficient turbulence and incoming solar radiation (K) less than 200 W m^{-2}, and summarized this at the 30-min timescale (86). Four eddy covariance towers were located in the Sierra Nevada around the upper Kings River basin along a west-to-east transect at $\sim$800 m elevation intervals beginning at 405 m. Four towers were located in the San Jacinto Mountains at elevations ranging from 205 m to 1710 m. One tower was located in the Santa Ana Mountains at $\sim$ 500 m. We calculated monthly GPP by integration after gap-filling intervals with missing, low turbulence, or otherwise unsuitable observations. All of the towers are well documented in the literature (41, 49).

To scale Landsat-observed NIRv to eddy covariance-measured GPP (39–42), we used a hybrid light use efficiency approach, in which the max NIRv–GPP relationship under optimal growing conditions was down-regulated with scalars of interpolated GRIDMET solar irradiance (88) (K) and PRISM temperature (84) (T). First, we calculate GPPmax using linear relationships between growing season NIRv (mean of nine upwind Landsat pixels adjacent to the tower) and GPP under peak growing season conditions. We defined peak growing season conditions as March, April, and May for shrub-dominated sites (AmeriFlux sites: CZ1, SCs, SCw, SCc, and SCd) and June, July, and August for tree-dominated sites (AmeriFlux sites: CZ2, CZ3, CZ4, and SCf). There was a strong association between monthly growing season NIRv and GPP ($r^2 = 0.703$). We computed downregulation scalars (0 to 1) based on the relationships of a GPP residual with solar radiation (K) and temperature (T) at each site to correct for K and T limitation on photosynthesis (*SI Appendix*, Fig. S9). We calculated the GPP residual by dividing the observed flux tower GPP by the NIRv predicted GPP. We filtered to include only observations with monthly NIRv predicted GPP values greater than 0.5. We calculated a third-degree polynomial fit for the nine flux tower sites to predict the monthly GPP residuals using T ($r^2 = 0.0938$). We calculated a linear fit to predict the monthly GPP residuals using K ($r^2 = 0.0553$). We multiplied these monthly T and K downregulation scalars by the GPPmax prediction at each site to get a final prediction of monthly GPP. Over all 90 site-years with twelve months of data, we get an r^2 of 0.86 between modeled and observed annual GPPs (*SI Appendix*, Fig. S10). We then applied the linear relationship between NIRv combined with the scalar corrections for K and T to convert monthly NIRv to GPP across California at 30-m spatial resolution.

FRAP Fire Polygon Dataset. To determine the timing and location of fires within California, we employed the Fire and Resource Assessment Program (FRAP) dataset (https://frap.fire.ca.gov/mapping/gis-data/), which contains more than a century of multiagency geospatial fire perimeters for California. The dataset was ingested into Google Earth Engine (78) and filtered for fires that occurred after 1919.

USFS Fire Severity Dataset. To determine the impact of fire severity on GPP recovery, we employed the USFS Vegetation Burn Severity dataset (https://www.fs.usda.gov/Internet/FSE_DOCUMENTS/fseprd596279.zip), which contains USFS fire perimeters from 1984 to 2017. Each fire is separated into up to four categories of pixel-wise fire severity (1 = unchanged, 2 = low severity, 3 = moderate severity, 4 = high severity) based on relative dNBR (RdNBR) (37). The RdNBR values are then calibrated to fire severity categories (89, 90). All pixels within each fire severity category are grouped into one polygon for each fire event, with up to four polygons for each fire.

Matched Controls. To compute the GPP impact of fire, we utilized a spatial control matching approach that takes into account interannual variability and the changing background climate and environmental conditions over the past century in California. Fire areas were matched with a group of pixels representing similar geographic and climatic characteristics to each fire. Each set of control pixels contained up to 200 pixels binned by latitude (0.25° bins), elevation (100-m bins), long-term mean precipitation (200-mm bins), and long-term mean temperature (5 °C bins) (*SI Appendix*, Fig. S2). Pixels were selected only if they did not occur in a recent fire (according to FRAP) and were otherwise not recently disturbed (since 1984, determined using the Continuous Change Detection and Classification algorithm) (29, 91). To check the fit, we regressed annual mean prefire GPP against the same year's mean control GPP, with an r^2 of 0.58 and an RMSE of 281.5 g C m^{-2} y^{-1} (*SI Appendix*, Fig. S8). We built an annual time series of GPP from the mean of these 200 control pixels. Each year of postfire GPP for each fire is compared to the same year's mean GPP for the matched control pixels. For example, a fire that burned in 2010 has its mean 2014 GPP (age = 4 y since fire) compared to the mean 2014 GPP of its 200 matched control pixels.

Uncertainty. We quantitatively propagate five sources of uncertainty in this analysis. They include

- NIRv–GPP empirical model fit (root mean squared error; *SI Appendix*, Fig. S10),
- spatial variability of fire polygon pixels (SE across all pixels that make up $GPP_{y,f}$),
- spatial variability of matched control pixels (SE across all pixels that make up $GPP_{y,cf}$),
- the quality of the spatial control match, measured by the linear fit of control pixels vs. observed project pixels, during the prefire period (root mean squared error; *SI Appendix*, Fig. S8), and
- variation in dGPP across the population of fires for any given year since fire (SE of the dGPP of each fire in a year since fire bin, $\overline{dGPP}_{ysf,fire_n}$).

Additional sources of uncertainty that are not explicitly treated are flux data processing (gap filling and partitioning into GPP) as well as the uncertainty in FRAP and USFS fire perimeters. We recognize that the fire perimeters pre-Landsat era, and especially the oldest fire perimeters, may be subject to error. It was out of scope for this paper to validate historic FRAP polygon accuracy (92).

To compute dGPP, we propagate the spatial error associated with the mean estimate of GPP for the fire pixels and the matched control pixels as well as root mean square error (RMSE) associated with the GPP model and control match:

$$dGPP_{y,f} = \overline{GPP}_{y,f} - \overline{GPP}_{y,c_f},$$

where y = year, f = fire, and c_f = matched control pixels for each fire. To compute the SE of $dGPP_{y,f}$:

$$SE(dGPP_{y,f}) = \sqrt{SE(\overline{GPP}_{y,f})^2 + SE(\overline{GPP}_{y,c_f})^2 + RMSE(GPP_{model})^2 + RMSE(ControlMatch)^2}.$$

To compute the dGPP for any given–year since fire–in the chronosequence, we take the mean of each fire's dGPP in a particular year since fire "bin":

$$dGPP_{ysf} = \overline{dGPP}_{ysf,f},$$

where ysf = years since fire. To compute the SE of $dGPP_{ysf}$,

$$SE(dGPP_{ysf}) = \sqrt{SE(\overline{dGPP}_{ysf,fire_1})^2 + SE(\overline{dGPP}_{ysf,fire_2})^2 + \ldots + SE(\overline{dGPP}_{ysf,fire_n})^2}/n_{fires}.$$

Data, Materials, and Software Availability. Code and data have been deposited at https://doi.org/10.5061/dryad.9w0vt4bkr.

ACKNOWLEDGMENTS. The Center for Ecosystem Climate Solutions is supported by California Strategic Growth Council's Climate Change Research Program (SGC CCR) with funds from California Climate Investments, a statewide initiative that puts billions of Cap-and-Trade dollars to work reducing greenhouse gas emissions, strengthening the economy, and improving public health and the environment–particularly in disadvantaged communities. K.S.H. was supported by California's SGC CCR under grant number CCR20021 and the Stanford Woods Institute for the Environment (all research was completed prior to joining Amazon Sustainability Science & Innovation). CAN was supported by the Ridge to Reef Graduate Training Program funded by NSF-NRT award DGE-1735040 and California's SGC CCR under grant number CCR20021. JAW was supported by California's SGC CCR under grant number CCR20021 and by the University of California's National Laboratories (UCNL) Laboratory Fees grant program under grant number LFR-18-542511.

Author affiliations: [a]Woods Institute for the Environment, Stanford University, Stanford, CA 92697; [b]Department of Earth System Science, University of California, Irvine, CA 92697; and [c]Department of Ecology and Evolutionary Biology, University of California, Irvine, CA 94305

1. F. Mouillot, C. B. Field, Fire history and the global carbon budget: A 1° × 1° fire history reconstruction for the 20th century. *Global Change Biol.* **11**, 398–420 (2005).
2. N. G. McDowell *et al*., Pervasive shifts in forest dynamics in a changing world. *Sci. (New York, N.Y.)* **368** (2020, in press).
3. P. Friedlingstein, Global carbon budget 2019. *Earth Syst. Sci. Data Discuss.* **11**, 1–79 (2019).
4. J. S. Landry, H. D. Matthews, Non-deforestation fire vs. fossil fuel combustion: The source of CO_2 emissions affects the global carbon cycle and climate responses. *Biogeosciences* **13**, 2137–2149 (2016).
5. G. R. Van Der Werf *et al*., Global fire emissions estimates during 1997–2016 (2017).
6. D. M. Bowman *et al*., Fire in the earth system (2009).
7. P. J. Grutzen, M. O. Andreae, Biomass burning in the tropics: Impact on atmospheric chemistry and biogeochemical cycles. *Science* **250**, 1669–1678 (1990).
8. G. B. Bonan, Forests and climate change: Forcings, feedbacks, and the climate benefits of forests. *Science (New York, N.Y.)* **320**, 1444–1449 (2008).
9. J. K. Agee, C. N. Skinner, Basic principles of forest fuel reduction treatments. *For. Ecol. Manag.* **211**, 83–96 (2005).
10. W. W. Covington, Helping western forests heal. *Nature* **408**, 135–136 (2000).
11. R. T. Brown, J. K. Agee, J. F. Franklin, Forest restoration and fire: Principles in the context of place. *Conserv. Biol.* **18**, 903–912 (2004).
12. R. K. Hagmann *et al*., Evidence for widespread changes in the structure, composition, and fire regimes of western North American forests. *Ecol. Appl.* **31**, e02431 (2021).
13. R. A. Minnich, M. G. Barbour, J. H. Burk, R. F. Fernau, Sixty years of change in Californian conifer forests of the San Bernardino mountains. *Conserv. Biol.* **9**, 902–914 (1995).
14. P. J. McIntyre *et al*., Twentieth-century shifts in forest structure in California: Denser forests, smaller trees, and increased dominance of oaks. *Proc. Natl. Acad. Sci. U.S.A.* **112**, 1458–1463 (2015).
15. A. A. Bernal, S. L. Stephens, B. M. Collins, J. J. Battles, Biomass stocks in California's fire-prone forests: Mismatch in ecology and policy. *Environ. Res. Lett.* **17**, 044047 (2022).
16. J. T. Abatzoglou, A. P. Williams, Impact of anthropogenic climate change on wildfire across western US forests. *Proc. Natl. Acad. Sci. U.S.A.* **113**, 11770–11775 (2016).
17. A. L. Westerling, Increasing western US forest wildfire activity: Sensitivity to changes in the timing of spring. *Philos. Trans. R. Soc. B: Biol. Sci.* **371**, 20150178 (2016).
18. C. Mallek, H. Safford, J. Viers, J. Miller, Modern departures in fire severity and area vary by forest type, Sierra Nevada and southern Cascades, California, USA. *Ecosphere* **4**, art153 (2013).
19. S. Liang, M. D. Hurteau, A. L. Westerling, Potential decline in carbon carrying capacity under projected climate-wildfire interactions in the Sierra Nevada. *Sci. Rep.* **7**, 2420 (2017).
20. B. M. Sleeter *et al*., Effects of 21st-century climate, land use, and disturbances on ecosystem carbon balance in California. *Global Change Biol.* **25**, 3334–3353 (2019).
21. J. S. Sperry *et al*., The impact of rising CO_2 and acclimation on the response of US forests to global warming. *Proc. Natl. Acad. Sci. U.S.A.* **116**, 25734–25744 (2019).
22. S. R. Coffield, K. S. Hemes, C. D. Koven, M. L. Goulden, J. T. Randerson, Climate-driven limits to future carbon storage in California's wildland ecosystems. *AGU Adv.* **2**, 1–18 (2021).
23. K. T. Davis *et al*., Wildfires and climate change push low-elevation forests across a critical climate threshold for tree regeneration. *Proc. Natl. Acad. Sci. U.S.A.* **116**, 6193–6198 (2019).
24. A. J. Tepley, J. R. Thompson, H. E. Epstein, K. J. Anderson-Teixeira, Vulnerability to forest loss through altered postfire recovery dynamics in a warming climate in the Klamath Mountains. *Global Change Biol.* **23**, 4117–4132 (2017).
25. W. D. Hansen, M. G. Turner, Origins of abrupt change? Postfire subalpine conifer regeneration declines nonlinearly with warming and drying. *Ecol. Monogr.* **89**, e01340 (2019).
26. J. D. Coop *et al*., Overview Articles Wildfire-Driven Forest Conversion in Western North American Landscapes (year?).
27. CalFire, Top 20 Largest California Wildfires (2019).
28. A. P. Williams *et al*., Observed impacts of anthropogenic climate change on wildfire in California. *Earth's Future* **7**, 892–910 (2019).
29. J. A. Wang, J. T. Randerson, M. L. Goulden, C. A. Knight, J. J. Battles, Losses of tree cover in California driven by increasing fire disturbance and climate stress. AGU Adv. **3**, e2021AV000654 (2022).
30. L. S. Adams, M. D. Nichols, J. N. Goldstene, "Climate Change Scoping Plan" First Update, (Tech. Rep. 2014).
31. CA-Air Resources Board, January 2019 DRAFT California Natural and Working Lands Climate Change Implementation Plan (Tech. Rep., 2019).
32. B. D. Amiro *et al*., Ecosystem carbon dioxide fluxes after disturbance in forests of North America. *J. Geophys. Res.: Biogeosci.* **115** (2010).
33. M. L. Goulden *et al*., Patterns of NPP, GPP, respiration, and NEP during boreal forest succession. *Global Change Biol.* **17**, 855–871 (2011).
34. B. E. Law, O. J. Sun, J. Campbell, S. Van Tuyl, P. E. Thornton, Changes in carbon storage and fluxes in a chronosequence of ponderosa pine. *Global Change Biol.* **9**, 510–524 (2003).
35. D. J. Young *et al*., Post-fire forest regeneration shows limited climate tracking and potential for drought-induced type conversion. *Ecology* **100**, 1–13 (2019).
36. K. B. Kemp, P. E. Higuera, P. Morgan, Fire legacies impact conifer regeneration across environmental gradients in the U.S. northern Rockies. *Landscape Ecol.* **31**, 619–636 (2016).
37. J. D. Miller, A. E. Thode, Quantifying burn severity in a heterogeneous landscape with a relative version of the delta Normalized Burn Ratio (dNBR). *Remote Sens. Environ.* **109**, 66–80 (2007).
38. J. Xiao *et al*., Remote sensing of the terrestrial carbon cycle: A review of advances over 50 years. *Remote Sens. Environ.* **233**, 111383 (2019).
39. G. Badgley, C. B. Field, J. A. Berry, Canopy near-infrared reflectance and terrestrial photosynthesis. *Sci. Adv.* **3**, e1602244 (2017).
40. G. Badgley, L. D. Anderegg, J. A. Berry, C. B. Field, Terrestrial gross primary production: Using NIRv to scale from site to globe. *Global Change Biol.* **122**, gcb.14729 (2019).
41. C. Hinojo-Hinojo, M. L. Goulden, Plant traits help explain the tight relationship between vegetation indices and gross primary production. *Remote Sens.* **12**, 1405 (2020).
42. D. D. Baldocchi *et al*., Outgoing near infrared radiation from vegetation scales with canopy photosynthesis across a spectrum of function, structure, physiological capacity and weather. *J. Geophys. Res. Biogeosci.* **125**, e2019JG005534 (2020).
43. E. Odum, The strategy of ecosystem development. *Science* **164**, 262–270 (1969).
44. California Air Resources Board, California Wildfire Emission Estimates (2020).
45. S. Dore *et al*., Long-term impact of a stand-replacing fire on ecosystem CO_2 exchange of a ponderosa pine forest. *Global Change Biol.* **14**, 1801–1820 (2008).
46. L. A. Cooper, A. P. Ballantyne, Z. A. Holden, E. L. Landguth, Disturbance impacts on land surface temperature and gross primary productivity in the western United States. *J. Geophys. Res.: Biogeosci.* **122**, 930–946 (2017).
47. D. Schimel, B. B. Stephens, J. B. Fisher, Effect of increasing CO_2 on the terrestrial carbon cycle. *Proc. Natl. Acad. Sci. U.S.A.* **112**, 436–441 (2015).
48. Z. L. Steel *et al*., Mega-disturbances cause rapid decline of mature conifer forest habitat in California. *Ecol. Appl.*, e2763 (2022).
49. M. L. Goulden, California forest die-off linked to multi-year deep soil drying in 2012–2015 drought. *Nat. Geosci.* **12**, 632–637 (2019).
50. A. F. Pellegrini *et al*., Fire frequency drives decadal changes in soil carbon and nitrogen and ecosystem productivity. *Nature* **553**, 194–198 (2018).
51. A. F. A. Pellegrini *et al*., Fire effects on the persistence of soil organic matter and long-term carbon storage. *Nat. Geosci.* **15**, 5–13 (2019).
52. M. J. Goodwin, M. P. North, H. S. Zald, M. D. Hurteau, Changing climate reallocates the carbon debt of frequent-fire forests. *Global Change Biol.* **26**, 6180–6189 (2020).
53. J. E. Stenzel *et al*., Fixing a snag in carbon emissions estimates from wildfires. *Global Change Biol.* **25**, 3985–3994 (2019).
54. M. C. Mack *et al*., Carbon loss from boreal forest wildfires offset by increased dominance of deciduous trees. *Science* **372**, 280–283 (2021).
55. M. E. Chambers, P. J. Fornwalt, S. L. Malone, M. A. Battaglia, Patterns of conifer regeneration following high severity wildfire in ponderosa pine - dominated forests of the Colorado Front Range. *For. Ecol. Manag.* **378**, 57–67 (2016).
56. C. W. Stephens, B. M. Collins, J. Rogan, Land ownership impacts post-wildfire forest regeneration in Sierra Nevada mixed-conifer forests. *For. Ecol. Manag.* **468**, 118161 (2020).
57. C. A. Knight *et al*., Land management explains major trends in forest structure and composition over the last millennium in California's Klamath Mountains. *Proc. Natl. Acad. Sci. U.S.A.* **119**, e2116264119 (2022).
58. California Forest Management Task Force, California's Wildfire and Forest Resilience Action Plan (Sacramento, Tech. rep., 2021).

59. S. L. Stephens, J. J. Moghaddas, B. R. Hartsough, E. E. Moghaddas, N. E. Clinton, Fuel treatment effects on stand-level carbon pools, treatment-related emissions, and fire risk in a Sierra Nevada mixed-conifer forest. *Can. J. For. Res.* **39**, 1538–1547 (2009).
60. J. L. Campbell, M. E. Harmon, S. R. Mitchell, Can fuel-reduction treatments really increase forest carbon storage in the western US by reducing future fire emissions? (2012).
61. J. Campbell, G. Alberti, J. Martin, B. E. Law, Carbon dynamics of a ponderosa pine plantation following a thinning treatment in the northern Sierra Nevada. *For. Ecol. Manag.* **257**, 453–463 (2009).
62. M. L. Wiechmann, M. D. Hurteau, M. P. North, G. W. Koch, L. Jerabkova, The carbon balance of reducing wildfire risk and restoring process: An analysis of 10-year post-treatment carbon dynamics in a mixed-conifer forest. *Clim. Change* **132**, 709–719 (2015).
63. D. J. Krofcheck, M. D. Hurteau, R. M. Scheller, E. L. Loudermilk, Prioritizing forest fuels treatments based on the probability of high-severity fire restores adaptive capacity in Sierran forests. *Global Change Biol.* **24**, 729–737 (2018).
64. S. L. Stephens *et al.*, The effects of forest fuel-reduction treatments in the United States. *BioScience* **62**, 549–560 (2012).
65. L. L. Yocom Kent *et al.*, Interactions of fuel treatments, wildfire severity, and carbon dynamics in dry conifer forests. *For. Ecol. Manag.* **349**, 66–72 (2015).
66. D. A. Jaffe, N. L. Wigder, Ozone production from wildfires: A critical review. *Atmos. Environ.* **51**, 1–10 (2012).
67. K. S. Hemes, J. Verfaillie, D. D. Baldocchi, Wildfire-smoke aerosols lead to increased light use efficiency among agricultural and restored wetland land uses in California's central valley. *J. Geophys. Res.: Biogeosci.* **125**, 1–21 (2020).
68. X. Yue, N. Unger, Fire air pollution reduces global terrestrial productivity. *Nat. Commun.* **9**, 5413 (2018).
69. N. Fann *et al.*, The health impacts and economic value of wildland fire episodes in the U.S.: 2008–2012. *Sci. Total Environ.* **610-611**, 802–809 (2017).
70. R. Rittmaster, W. L. Adamowicz, B. Amiro, R. T. Pelletier, Economic analysis of health effects from forest fires. *Can. J. For. Res.* **36**, 868–877 (2006).
71. Y. Jin, J. T. Randerson, M. L. Goulden, S. J. Goetz, Post-fire changes in net shortwave radiation along a latitudinal gradient in boreal North America. *Geophys. Res. Lett.* **39**, n/a (2012).
72. Z. Liu, A. P. Ballantyne, L. A. Cooper, Biophysical feedback of global forest fires on surface temperature. *Nat. Commun.* **10**, 214 (2019).
73. F. N. N. Robinne *et al.*, A spatial evaluation of global wildfire-water risks to human and natural systems. *Sci. Total Environ.* **610–611**, 1193–1206 (2018).
74. H. G. Smith, G. J. Sheridan, P. N. Lane, P. Nyman, S. Haydon, Wildfire effects on water quality in forest catchments: A review with implications for water supply (2011).
75. F. Z. Maina, E. R. Siirila-Woodburn, Watersheds dynamics following wildfires: Nonlinear feedbacks and implications on hydrologic responses. *Hydrol. Process.* hyp.13568 (2019).
76. R. B. Walker, J. D. Coop, S. A. Parks, L. Trader, Fire regimes approaching historic norms reduce wildfire-facilitated conversion from forest to non-forest. *Ecosphere* **9**, e02182 (2018).
77. E. L. Kalies, L. L. Yocom Kent, Tamm review: Are fuel treatments effective at achieving ecological and social objectives? A systematic review (2016).
78. N. Gorelick *et al.*, Google earth engine: Planetary-scale geospatial analysis for everyone. *Remote Sens. Environ.* **202**, 18–27 (2017).
79. D. P. Roy *et al.*, Characterization of Landsat-7 to Landsat-8 reflective wavelength and normalized difference vegetation index continuity. *Remote Sens. Environ.* **185**, 57–70 (2016).
80. M. A. Wulder, J. G. Masek, W. B. Cohen, T. R. Loveland, C. E. Woodcock, Opening the archive: How free data has enabled the science and monitoring promise of Landsat. *Remote Sens. Environ.* **122**, 2–10 (2012).
81. Z. Zhu, S. Wang, C. E. Woodcock, Improvement and expansion of the Fmask algorithm: Cloud, cloud shadow, and snow detection for Landsats 4–7, 8, and Sentinel 2 images. *Remote Sens. Environ.* **159**, 269–277 (2015).
82. E. P. Crist, R. C. Cicone, A physically-based transformation of thematic mapper data-The TM tasseled cap. *IEEE Trans. Geosci. Remote Sens.* **GE-22**, 256–263 (1984).
83. C. Key, N. Benson, "Landscape assessment: Remote sensing of severity, the Normalized Burn Ratio" in *FIREMON: Fire effects monitoring and inventory system. General Technical Report, RMRS-GTR-164-CD:LA1-LA51*, D. C. Lutes, Ed. (USDA Forest Service, Rocky Mountain Research Station., Ogden, UT, 2005).
84. C. Daly *et al.*, Physiographically sensitive mapping of climatological temperature and precipitation across the conterminous United States. *Int. J. Climatol.* (2008).
85. S. Hooper, R. E. Kennedy, A spatial ensemble approach for broad-area mapping of land surface properties. *Remote Sens. Environ.* **210**, 473–489 (2018).
86. M. L. Goulden *et al.*, Evapotranspiration along an elevation gradient in California's Sierra Nevada. *J. Geophys. Res.: Biogeosci.* **117**, 1–13 (2012).
87. M. L. Goulden *et al.*, An eddy covariance mesonet to measure the effect of forest age on land-atmosphere exchange. *Global Change Biol.* **12**, 2146–2162 (2006).
88. J. T. Abatzoglou, Development of gridded surface meteorological data for ecological applications and modelling. *Int. J. Climatol.* **33**, 121–131 (2013).
89. J. D. Miller *et al.*, Calibration and validation of the relative differenced Normalized Burn Ratio (RdNBR) to three measures of fire severity in the Sierra Nevada and Klamath Mountains, California, USA. *Remote Sens. Environ.* **113**, 645–656 (2009).
90. J. D. Miller, B. Quayle, Calibration and validation of immediate post-fire satellite-derived data to three severity metrics. *Fire Ecol.* **11**, 12–30 (2015).
91. Z. Zhu, C. E. Woodcock, Continuous change detection and classification of land cover using all available Landsat data. *Remote Sens. Environ.* **144**, 152–171 (2014).
92. A. D. Syphard, J. E. Keeley, Historical reconstructions of California wildfires vary by data source. *Int. J. Wildland Fire* **25**, 1221–1227 (2016).